Environmental dependence of preresonance Raman cross-section dispersions: Benzene vapor-phase excitation profiles

Paul A. Harmon and Sanford A. Asher
Chemistry Department, University of Pittsburgh, Pittsburgh, Pennsylvania 15260

(Received 12 April 1990; accepted 18 May 1990)

The vapor-phase Raman cross-section excitation profiles of the two totally symmetric modes of benzene have been measured between 514 and 220 nm. At wavelengths longer than 280 nm, the 992 cm^{-1} ν_1 ring breathing-mode cross-section dispersion is not indicative of preresonance enhancement by the dipole-allowed E_{1u} electronic transition near 185 nm. With excitation wavelengths shorter than 240 nm, however, the ν_1 mode dispersion is dominated by enhancement from the B_{1u}/E_{1u} state. The ν_2 3060 cm^{-1} carbon–hydrogen stretching vibration shows no enhancement by the E_{1u} state in the 514–220 nm spectral region. The cross-section dispersion is indicative of enhancement by states centered near 100 000 cm^{-1}. We compare the gas- and condensed-phase Raman cross-section dispersions of benzene, cyclohexane, and acetonitrile. Surprisingly, we do not observe the "extra" dispersion predicted to occur in the condensed phase which derives from the dispersion in the local electromagnetic field strength.

I. INTRODUCTION

The excitation frequency dependence of preresonance Raman cross sections obtained with excitation energies below that of the lowest dipole-allowed singlet electronic transitions, have provided important tests for Raman scattering theory. The preresonance frequency dependences have generally been analyzed in terms of the vibronic theory of Raman scattering using the formalisms developed by Albrecht *et al.*[1-3] This preresonance theory concludes that those vibrational modes which have the largest enhancements from the lowest-energy electronic transitions will show the largest dispersions in their Raman cross sections as the excitation frequency moves further into the UV region. The preresonance Raman cross-section excitation profiles can therefore be used to determine which electronic transitions contribute to the enhancement of particular vibrational modes. In fact, the preresonance Raman cross-section dispersions of a variety of molecules and ions such as NO_3^-, SO_4^{2-}, cacodylate, water, acetonitrile, acetone, N-methyl acetamide, cyclohexane, benzene, and benzene derivatives have been analyzed using this vibronic formalism.[4-9]

These preresonance studies of Raman cross-section dispersions have been carried out almost entirely in the condensed phase, and it has been assumed that condensed-phase cross-section dispersions monitor those electronic properties characteristic of the isolated molecule. The dispersion in the local electromagnetic field strength in the condensed phase, however, should lead to increased dispersions compared to those of the isolated molecule. This "extra" dispersion derives from the modulation of the incident and scattered electromagnetic fields through the wavelength-dependent dielectric constant or refractive index of the condensed-phase medium.[10-14] Solvent perturbation of molecular excited states, leading to different preresonance frequency dependences, are also possible but have not been explicitly considered. These types of effects can only be revealed by comparing the vapor-phase and condensed-phase Raman cross-section dispersions of the same molecule. This has not been possible previously due to the few vapor-phase cross-section dispersion studies completed.[14]

We report here detailed vapor-phase cross-section dispersion studies of the totally symmetric modes of benzene between 514 and 220 nm. Benzene vapor cross sections are compared to the numerous previous condensed-phase benzene cross-section studies.[7-9] We have extended condensed-phase benzene ν_2 3060 cm^{-1} carbon–hydrogen stretching cross-section measurements to 230 nm. We also measure and compare the dispersion of the Raman cross sections of liquid- and vapor-phase acetonitrile and cyclohexane at several wavelengths between 514 and 230 nm.

We discuss initially our vapor-phase benzene 992 cm^{-1} ν_1 and 360 cm^{-1} ν_2 cross sections in terms of the Albrecht formalism and we compare the condensed- and vapor-phase dispersions. These dispersions are identical, in sharp contrast to the theoretically predicted increased condensed-phase dispersions expected from the dispersion in the local electromagnetic field strength. The results here indicate that a reevaluation of the local-field model is necessary for interpreting measured Raman cross sections and their dispersion in the condensed phase.

II. EXPERIMENT

Raman spectra were measured using instrumentation described in detail elsewhere.[15] Excitation wavelengths of 514, 488, and 457 nm were derived from a Spectra Physics model 164 argon-ion laser. The remaining excitation wavelengths were generated by a Quanta-Ray DCR-2A Nd:YAG laser (where YAG denotes yttrium aluminum garnet) operated at 20 Hz and frequency doubled to pump a dye laser. Excitation at 377 and 400 nm was obtained by mixing the dye laser light with the 1.06 μm Nd:YAG fundamental, 280–320 nm excitation was generated by doubling the dye-laser output, while 235–217 nm excitation was derived from mixing the Nd:YAG fundamental with the doubled dye-laser output. The scattered light was collected at 90° by reflective optics in order to avoid chromatic aberrations. A crys-

 0021-9606/90/173094-07$03.00

talline quartz polarization scrambler was used to remove any polarization efficiency bias of the monochromator. A Spex Triplemate monochromator was used to disperse the scattered light which was detected by a PAR OMA II system equipped with a PAR 1420 blue-enhanced intensified Reticon detector. The monochromator and detector efficiencies were determined between 700 and 400 nm by using a tungsten–halogen standard intensity lamp, and between 400 and 200 nm by using a deuterium standard intensity lamp (Optronic Laboratories, models 550 and UV-40, respectively). The light from the standard lamps was scattered off a $BaSO_4$ Lambert surface and imaged onto the entrance slit of the monochromator.

Vapor-phase Raman spectra were obtained in an open flowing system. Research grade methane (Burrell Industries) flowed through two successive bubblers containing liquid benzene (Baker) to saturate the methane gas with benzene vapor. The benzene reservoirs were held at a constant temperature several degrees below room temperature (22 ± 0.5 °C). The gaseous mixture of 80 Torr benzene and 680 Torr methane flowed through a cylindrical nozzle ~ 1 mm wide and 20 mm long. A nitrogen purge surrounded the gaseous mixture. Excitation occurred ~ 1 mm from the nozzle tip, and the vapor was exhausted to a hood by an aspirator. The benzene ν_1 992 cm^{-1} ring breathing-mode and the ν_2 3060 cm^{-1} carbon–hydrogen stretching-mode Raman cross-section dispersions were measured relative to the 2920 cm^{-1} carbon–hydrogen (C–H) stretching vibration of methane. The excitation frequency dependence of the 2920 cm^{-1} band of methane has been measured directly between 600 and 200 nm by Black and Bischel.[16] For excitation wavelengths longer than 300 nm, the benzene 992 cm^{-1} and methane 2920 cm^{-1} bands could not be simultaneously imaged onto the detector; successive Raman measurements were made monitoring the power before and after each measurement.

The Raman cross-section dispersions of the 2900–3100 cm^{-1} C–H stretching vibration of liquid acetonitrile and the 2800–3000 cm^{-1} C–H stretching vibrations of liquid cyclohexane were directly measured at several wavelengths using the method outlined in detail by Dudik, Johnson, and Asher.[4] In this method, Raman intensities are normalized to the laser intensity within the scattering volume by measuring the Raman intensities as well as the intensity of the laser light scattered from a dispersion of $BaSO_4$ particles in the liquid samples. Changes in the Raman-scattered intensity relative to the scattered laser light intensity as a function of wavelength then reflect the dispersion in the Raman cross sections.

The vapor- and condensed-phase data each derive from at least three measurements with relative standard deviations of $\sim 5\%$. In all cases the Raman cross sections were calculated from peak area measurements because significant differences in vibrational band shapes are obvious.

III. RESULTS

Table I gives the benzene gas-phase 992 cm^{-1} and 3060 cm^{-1} 90° differential Raman cross sections measured here between 514 and 217 nm. Our 992 cm^{-1} vapor-phase cross sections agree with the few previously measured 992 cm^{-1} gas-phase cross-section data. Udagawa *et al.*[17] measured the 992 cm^{-1} vapor cross section at 514 and 337 nm to be 7.5 and 65 μb/sr, respectively. Our 992 cm^{-1} cross section of 7.1 μb/sr at 514 nm is consistent with the measurement of Udagawa *et al.* The least-squares fit to our 992 cm^{-1} cross sections (see below) between 514 and 280 nm predicts a cross section of 70 μb/sr at 337 nm which agrees well with the results of Udagawa *et al.* No previous vapor-phase Raman cross-section data for the benzene ν_2 3060 cm^{-1} C–H stretching band have been reported to our knowledge.

TABLE I. Benzene vapor ν_1 and ν_2 cross sections. Cross section units are 10^{-30} cm^2/mol Sr (μb/mol sr).

λ_{ex}	$d\sigma/d\Omega$, 992 cm^{-1} gas	$d\sigma/d\Omega$, 3060 cm^{-1} gas
514	7.1	12
488	8.7	16
457	12	22
400	28	44
320	100	150
280	250	310
235	1500	790
230	2500	1000
225	3800	1200
220	6500	
217	9400	

Figures 1 and 2 show plots of the 992 and 3060 cm^{-1} vapor cross sections between 514 and 217 nm. The data between 514 and 320 nm are also displayed on an expanded ordinate scale, to facilitate a sensitive comparison between the measured data and the fitted solid curves. Also displayed in the lower portion of each figure is the benzene vapor absorption spectrum in the same spectral region. The structure in the vapor absorption spectrum between $\sim 36\,000$ and 45 000 wave numbers is due to vibronic components of the forbidden transition to the $^1B_{2u}$ electronic state. The onset of the sharply rising absorption near 46 000 cm^{-1} derives from the red edge of the stronger transitions to the $^1B_{1u}$ and partially overlapping $^1E_{1u}$ electronic states. The data shown in

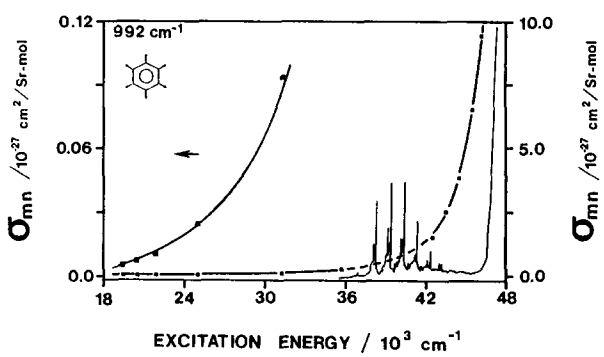

FIG. 1. Benzene gas-phase Raman excitation profile of the 992 cm^{-1} ring breathing mode from 514 to 217 nm. Upper curve ordinate scaling is indicated on the left-hand side of the figure. A benzene gas-phase absorption spectrum is also shown. The dashed curve between 36 000 and 42 000 cm^{-1} exists to remind the reader that narrow excitation profile features would occur upon excitation within the narrow B_{2u} vibronic features (Refs. 9 and 18).

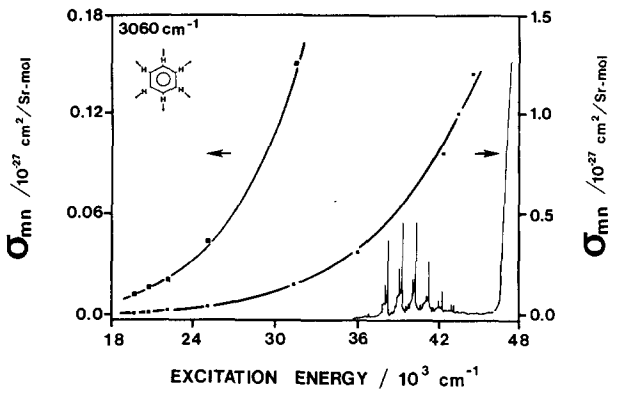

FIG. 2. Benzene gas-phase excitation profile of the 3060 cm^{-1} carbon–hydrogen stretching vibration. Expanded ordinate scaling is indicated on the left-hand side. Note the reduced slope of the lower curve in the 36 000–45 000 cm^{-1} region compared to that in Fig. 1.

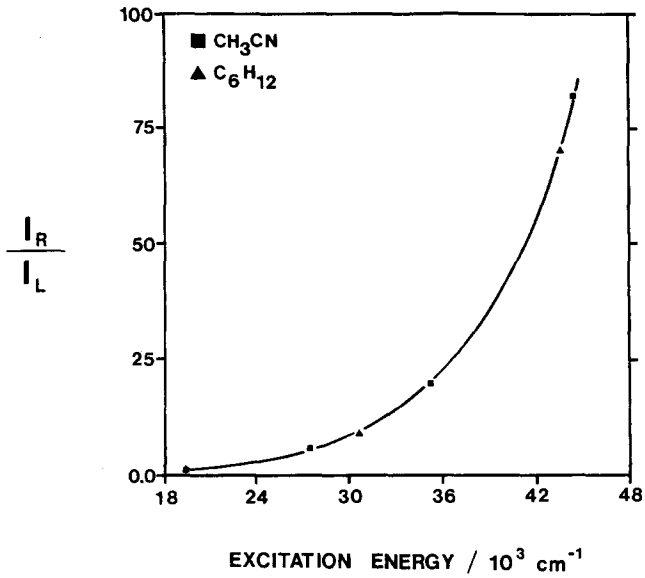

FIG. 3. Excitation frequency dependence of the relative Raman intensities I_R of the 2900–3100 cm^{-1} acetonitrile mode (squares) and the 2800–3000 cm^{-1} cyclohexane bands (triangles) referenced to the elastically scattered laser line intensity I_L. The I_R/I_L values are normalized to one at 514 nm.

Figs. 1 and 2 are not in resonance with any of the narrow vibronic bands of the $^1B_{2u}$ transition. Resonance with these features would result in the strong enhancement of the 992 cm^{-1} intensity as well as overtones and combination bands. In a recent report,[18] we utilized interferences between the preresonance enhancement of the 992 cm^{-1} mode and the resonant $^1B_{2u}$ state enhancement to examine the nature of the resonance emission from high-energy vapor-phase $^1B_{2u}$ vibronic levels.

The 992 cm^{-1} cross sections tabulated in Table I and displayed in Fig. 1 increase as the excitation energy nears the $^1B_{1u}/^1E_{1u}$ electronic states. The 3060 cm^{-1} C–H stretching mode, however, increases much more slowly and does not appear to be enhanced by the $^1B_{1u}/^1E_{1u}$ electronic states. This is evident by comparison of the slopes of the 992 and 3060 cm^{-1} cross-section plots in the ~40 000–45 000 wave number region in Figs. 1 and 2. Between 280 and 220 nm, for example, the 992 cm^{-1} mode cross section increases by ~26 while the 3060 cm^{-1} band increases only a factor of ~4. It should be pointed out, however, that the 3060 cm^{-1} mode dispersion is significantly greater than a simple $\nu_0\nu_s^3$ frequency dependence which would increase the 3060 cm^{-1} Raman cross section by 40-fold from 514 to 225 nm; we measure a 100-fold increase.

Figure 3 shows the excitation frequency dependence of the Raman intensities of the 2900–3000 cm^{-1} and 2800–3000 cm^{-1} C–H stretching bands of liquid acetonitrile and liquid cyclohexane, respectively, divided by the intensity of the elastically scattered laser line. The lowest-energy intensity ratios at 514 nm have been normalized to one in both cases. We have scaled these ratios to remove the very weak dependence of the elastic scattering from the $BaSO_4$ on the excitation energy.[4] Figure 3 shows that both the acetonitrile and cyclohexane C–H stretching cross sections increase by a factor of ~70 between 514 and 230 nm. These similar dispersions are consistent with the expectation of essentially identical enhancements for $\sigma^* \leftarrow \sigma$ type excitations in the deep ultraviolet region for all aliphatic C–H vibrations.

Figure 4 shows the dispersion of the ν_2 3060 cm^{-1} C–H stretching-mode Raman cross section of benzene in acetonitrile solution (40% benzene by volume). The 3060 cm^{-1} dispersion in Fig. 4 derives from measurements of the relative Raman intensity ratios between the benzene 3060 cm^{-1} and the acetonitrile 2900–3000 cm^{-1} bands. We have assumed in Fig. 4 that the 2900–3000 cm^{-1} acetonitrile mode Raman cross-section dispersion in a solution of benzene and acetonitrile is identical to the cross-section dispersion we directly measure in Fig. 3 for pure acetonitrile. The absolute cross-section scaling in Fig. 4 derives from absolute cross-section measurements by other workers at 514 nm. This can be accomplished by several different approaches. For example, the value of the 3060 cm^{-1} cross section of neat benzene at 514 nm, which was measured to be 45 μb/sr by Schomaker, Delaney, and Champion,[8] can then be scaled using

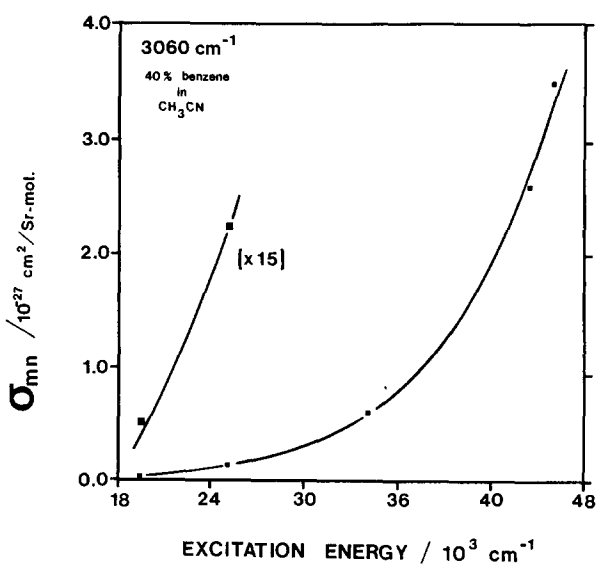

FIG. 4. Excitation profile of the 3060 cm^{-1} benzene mode in 40% benzene in acetonitrile from 514 to 225 nm. The two lowest-energy data are also displayed on an expanded scale.

the local-field correction (see below) to the solution composition used in Fig. 4 to give a 3060 cm^{-1} cross section of 37 μb/sr at 514 nm. Alternatively, we can use the 918 cm^{-1} C–C stretching cross section of pure acetonitrile of 1.2 μb/sr (Refs. 4 and 8) at 514 nm and our measurement of the (2900–3000 cm^{-1})/918 cm^{-1} integrated Raman intensity ratio of 13.2 to calculate a 2900–3000 cm^{-1} cross section of $\sim 16\,\mu$b/sr in pure acetonitrile. This value can then be scaled to 40% benzene in acetonitrile to give a 3060 cm^{-1} cross section of 34 μb/sr at 514 nm. We choose to use the value of Schomaker, Delaney, and Champion[8] to scale Fig. 4 as it is a more direct approach. Since we are concerned ultimately here with the dispersions in the cross sections, the normalization to absolute cross-section values at 514 nm will have no impact on our conclusions.

IV. DISCUSSION

A. Vapor-phase preresonance Raman cross-section dispersions

In the vapor phase the frequency dependence of the Raman cross section, σ_{nm}, of the Raman vibrational transition $n \leftarrow m$ can be described by

$$\sigma_{mn}(\nu_0) = K\nu_0(\nu_s)^3 \sum_{\rho,\sigma} |\alpha_{\rho,\sigma}(\nu_0)|^2, \tag{1}$$

where ν_0 is the excitation frequency (cm^{-1}). $\nu_s = \nu_0 - \nu_{mn}$, where ν_{mn} is the frequency of the vibrational mode and K stands for a collection of constants independent of ν_0. $\alpha_{\rho\sigma}(\nu_0)$ is the ρ,σth component ($\rho,\sigma = x,y,z$) of the Raman polarizability tensor for excitation at ν_0. The components of the polarizability tensor are given by[3]

$$\alpha_{\rho,\sigma} = \sum_{ev} \frac{\langle gn|R_\sigma|ev\rangle\langle ev|R_\rho|gm\rangle}{\nu_{ev} - \nu_m - \nu_0 - i\Gamma_e} + \frac{\langle gm|R_\rho|ev\rangle\langle ev|R_\sigma|gn\rangle}{\nu_{ev} - \nu_n + \nu_0 - i\Gamma_e}. \tag{2}$$

R_σ is the electric dipole moment operator along the molecular coordinate σ. ν_m and ν_n are the frequencies of the initial and final vibrational levels of the ground electronic state g, and ν_{ev} is the vibronic transition frequencies from the initial state to a particular vibronic level of the excited electronic state $|e\rangle$. The summation is over all molecular excited states except the ground state. Γ_e is the damping factor associated with each excited state $|e\rangle$.

Rigorous summation over all $|e\rangle$ is obviously difficult for all but the simplest molecules. The Albrecht A-term approximation[1-3] to the preresonance excitation frequency dependence of $\alpha_{\rho,\sigma}$ has been widely utilized to characterize preresonance Raman dispersions of totally symmetric vibrations. The derivation of this expression has its basis in the vibronic theory of Raman scattering, and considers a single dipole-allowed electronic transition to dominate the summation over all ev in Eq. (2). The A-term expression for the preresonance frequency dependence of σ_{mn} in the vapor phase is

$$\sigma_{mn}(\nu_0) = K_1\nu_0\nu_s^3\left[\frac{\nu_e^2 + \nu_0^2}{(\nu_e^2 - \nu_0^2)^2} + K_2\right]^2, \tag{3}$$

where K_1 is a constant independent of ν_0, proportional to the square of the oscillator strengths of the excited state(s) giving rise to the enhancement. ν_0 and ν_s are as defined in Eq. (1). When $K_2 = 0$, Eq. (3) is the simple A-term expression and the dispersion is modeled as deriving from a single state or states with transition energy ν_e. Nonzero values of K_2 model the contribution of an additional electronic state at sufficiently high frequency as to give a frequency-independent contribution to the Raman polarizability. In cases where at least two electronic states with different transition frequencies are important, this "modified" A-term expression dramatically improves modeling of the preresonance Raman data. The value of ν_e derived from fitting Eq. (3) to σ_{mn} values measured as a function of ν_0 should, in principle, correspond to the transition energy of a dipole-allowed electronic transition. Far from resonance, however, fitted values of ν_e are likely to reflect some weighted contribution of states with different transition energies.

The dramatic differences in the vapor excitation profiles for the ν_1 ring-breathing and ν_2 C–H stretching vibrations of benzene reflect the different energies of the important preresonance electronic transitions from which these modes derive intensity. The curves drawn through the 514–320 nm data on the expanded cross-section axes in Figs. 1 and 2 show the simple A-term best fits to the ν_1 and ν_2 cross-section dispersions between 514 and 280 nm. For the 514–280 nm region the best-fit curve to the 992 cm^{-1} ν_1 cross-section data in Fig. 1 is given by $K_2 = 0$, $K_1 = 1.1\times10^{-27}$ cm^2/mol, and a far ultraviolet transition energy of $\nu_e = 74\,000$ cm^{-1} (135 nm). This clearly indicates that the dipole-allowed $\pi^* \leftarrow \pi$ transition to the $^1E_{1u}$ electronic state at $\sim$190 nm does not dominate the ν_1 992 cm^{-1} dispersion at excitation wavelengths longer than 280 nm. The analogous curve in Fig. 2 shows the best fit to the ν_2 3060 cm^{-1} data over the 514–280 nm spectral range. This curve is given by $K_2 = 0$, $K_1 = 1.2\times10^{-26}$ cm^2/mol and a transition energy of $\nu_e = 100\,000$ cm^{-1} (100 nm). This ν_e value indicates enhancement for the 3060 cm^{-1} mode is dominated by higher-energy electronic states than the 992 cm^{-1} mode.

The curve in Fig. 1 through all the 992 cm^{-1} cross-section data derives from the modified A-term best fit to all the data between 514 and 217 nm with the best-fit parameters of $K_1 = 1.0\times10^{-29}$ cm^2/mol, $K_2 = 1.97\times10^{-9}$ cm^2, and $\nu_e = 52\,000$ (192) nm. This value of ν_e for the lower-energy active electronic transition is in good agreement with the transition energies to the $^1B_{1u}$ and $^1E_{1u}$ electronic states of 206 and 177 nm, respectively, and indicates that the 992 cm^{-1} mode is enhanced mainly by these transitions at excitation wavelengths to the blue of the forbidden $^1B_{2u}$ electronic states. Similar enhancement of the 992 cm^{-1} mode by the $^1B_u/^1E_u$ electronic states in this spectral region for a solution of 1% benzene in acetonitrile were reported previously by Asher and Johnson.[9] It should be noted that a simple A-term description of the 992 cm^{-1} data between 514 and 217 nm results in a poor fit which systematically underestimates the >280 nm data by as much as 40%, while the data in the <280 nm region are significantly overestimated. The simple A-term expression, which models one contributing electronic state, cannot simultaneously de-

scribe the 514–280 nm dispersion and the 240–217 nm dispersion.

The simple A-term fit to the 3060 cm^{-1} vapor cross section between 514 and 225 nm is shown in Fig. 2. The simple A-term expression adequately models the data, nonzero values of K_2 do not significantly change the fits. The A-term parameters are $K_2 = 0$, $K_1 = 1.4 \times 10^{-26}$ cm^2/mol, and $\nu_e = 104\,000$ (108 nm). The dispersion of the 3060 cm^{-1} mode throughout the visible spectral region to 225 nm is completely described by transitions centered around 100 000 cm^{-1}. This C–H stretching vibration shows no Raman cross-section enhancement from the dipole-allowed $^1E_{1u}$ or the $^1B_{1u}$ electronic states.

The dramatic difference between the ν_1 992 cm^{-1} C–C ring breathing-mode dispersion and the ν_2 3060 cm^{-1} C–H stretching-mode dispersion at wavelengths shorter than ~250 nm reflects the fact that the electronic and geometry changes occurring from the $\pi \leftarrow \pi$ transitions to the $^1B_{1u}$ and $^1E_{1u}$ excited states is restricted to the benzene C–C ring framework. The transition to the $^1B_{1u}$ and $^1E_{1u}$ states does not perturb the C–H bond lengths or force constants.

An energy of ~100 000 for an electronic transition that is important for the dispersion of the C–H stretching vibration may be reasonable in view of the Koch and Otto[19] synchrotron far-UV benzene study which characterized three ionization energies at 108 000, 124 000, and 132 000 cm^{-1} for electrons originating in sigma orbitals associated with C–H bonding. Any $\sigma^* \leftarrow \sigma$ transitions involving these orbitals would occur at a somewhat lower energy. Our vapor-phase 3060 cm^{-1} dispersions may suggest that the C–H stretching vibration derives its enhancement from these transitions.

B. Comparison between vapor- and condensed-phase Raman dispersions

Differences in vapor- and condensed-phase preresonance Raman cross-section dispersions could derive from two sources. The first is a difference in $\alpha_{\rho,\sigma}$ in Eqs. (1) and (2), and in ν_e in Eq. (3), in the condensed phase versus the gas phase due to solvent perturbations of the excited electronic states of the scattering molecule. For example, most electronic transitions are broadened in condensed phases compared to the vapor phase and are usually shifted slightly in energy. In the preresonance spectral regions where Eq. (3) is valid, we expect these changes to alter the σ_{mn} cross-section dispersion only in the case where the change in ν_e is significant compared to the energy difference $\nu_e - \nu_0$. In Eq. (3), broadening will not change the value of ν_e since the average transition energy remains the same, nor will it even affect the frequency-independent value of K_1 since the integrated oscillator strengths are not reduced. It is possible that $\alpha_{\rho,\sigma}$ and ν_e in Eq. (3) could be altered by changes in the nature of electronic transitions in the condensed versus the vapor phase. In cases where Rydberg transitions are extensively mixed with valence transitions, for example, it is known that solvation can decouple these transitions to result in transitions in the liquid which are more purely valence in character.[20] On the other hand, the valence character of certain high-energy transitions could decrease in the condensed phase, with the solvent providing acceptor orbitals for charge-transfer-like solvent–solute transitions. Differences in the preresonance dispersions between the gas and liquid will result only if these types of perturbations change the relative contribution to the intensity enhancement of different electronic transitions.

The second factor leading to differences in condensed-phase versus vapor-phase Raman cross-section dispersions, which is expected to be universal, derives from the dispersion in the "local field" for scattering in condensed phases. The local-field effect originates from the increased amplitude of the incident and Raman-scattered electric fields due to the dielectric nature of the condensed-phase scattering medium. The local-field correction predicts that the ratio of the Raman cross section of a solute molecule dissolved in a solvent, to that of the solute vapor, is given by[10–13]

$$\frac{\sigma_{mn}^{(\text{solution})}}{\sigma_{mn}^{(\text{vapor})}} = L(\nu_0) = \frac{n'_{\text{sol}}(\nu_0)}{n_{\text{sol}}(\nu_0)} \left\{ \frac{n^2(\nu_0) + 2}{[n/n_{\text{sol}}(\nu_0)]^2 + 2} \right\}^2 \times \left\{ \frac{(n')^2(\nu_0) + 2}{[n'/n'_{\text{sol}}(\nu_0)]^2 + 2} \right\}^2 \tag{4}$$

where $n(\nu_0)$ and $n'(\nu_0)$ represent the refractive index of pure liquid solute (scatterer) at the excitation frequency ν_0 and at the Raman-scattered frequency, respectively. $n_{\text{sol}}(\nu_0)$ and $n'_{\text{sol}}(\nu_0)$ are the refractive indices of the solution at the excitation frequency and the Raman-scattered frequency, respectively. It is worthwhile to point out, as Fini, Mirone, and Patella[11] did originally, that only in the case of pure liquids, when the solute and solvent are identical, does Eq. (4) reduce to

$$L(\nu_0) = \left[\frac{n^2(\nu_0) + 2}{3} \right]^4 \tag{5}$$

if the difference between $n'(\nu_0)$ and $n(\nu_0)$ as well as between $n'_{\text{sol}}(\nu_0)$ and $n_{\text{sol}}(\nu_0)$ is considered negligible. Numerous Raman studies in the visible[10–14] spectral region have shown that Eqs. (4) and (5) adequately describe the measured differences between vapor and pure liquid cross sections, as well as the dependence of the solute cross section on the refractive index of the solvent.

The local-field correction as given in Eqs. (4) and (5) should give "extra" dispersion in the condensed phase over that observed in the vapor phase due to the dispersion in the refractive indices n, n', n_{sol}, and n'_{sol} throughout the visible and ultraviolet spectral regions. Table II shows the calculated local-field corrections at 514, 325, and 230 nm for the C–H stretching bands of pure liquid benzene (L_B), acetonitrile (L_A), and cyclohexane (L_C), as well as for benzene in a solution 40% by volume benzene in acetonitrile (L_{BA}) and for acetonitrile in a solution of 40% benzene in acetonitrile (L_{AB}). The dispersion in the local-field correction between 230 and 514 nm should therefore give additional dispersions of $3.04/2.64 = 1.15$, $4.03/3.30 = 1.22$, and $7.07/4.08 = 1.73$ for liquid acetonitrile, cyclohexane, and benzene, respectively, compared to those in the vapor phase.

Our vapor-phase benzene ν_1 and ν_2 cross-section dispersions can be compared to those of condensed-phase neat benzene reported by Schomaker, Delaney, and Champion[8] to directly examine local-field dispersion effects as well as possible changes in $\alpha_{\rho,\sigma}$. Schomaker, Delaney, and Champion[8]

TABLE II. Refractive indices of benzene (n_B), acetonitrile (n_A), and cyclohexane (n_C) at 514, 315, and 230 nm. Local-field calculated ratio of condensed/vapor-phase Raman cross-section ratios from Eqs. (4) or (5) for pure benzene (L_B), pure acetonitrile (L_A), pure cyclohexane (L_C), 40% benzene in acetonitrile, benzene as scatterer (L_{BA}), 40% benzene in acetonitrile, acetonitrile as scatterer (L_{AB}).

λ_{ex}	n_B	n_A	n_C	L_B	L_A	L_C	L_{BA}	L_{AB}
514	1.51[a]	1.35[a]	1.43[b]	4.08	2.64	3.30	3.34	2.90
325	1.58[a]	1.37[a]	1.47[b]	4.84	2.78	3.70	4.20	3.22
230	1.79[b]	1.40[c]	1.50[b]	7.07	3.04	4.03	5.40	4.00

[a] Refractive indices measured by Shomaker, Delaney,and Champion (Ref. 8).
[b] Refractive indices measured by Sowers *et al.* (Ref. 21).
[c] Extrapolated index from measurements of Shomaker, Delaney, and Champion (Ref. 8).

compiled previous liquid-benzene ν_1 992 cm^{-1} cross-section data between 647 and 337 nm and compared these data to their own measurements between 514 and 325 nm. A-term calculated dispersions were compared to these data by normalizing the calculated curves to the average value of the neat 992 cm^{-1} cross section at 514 nm, as measured by five independent workers. Comparison of these curves to the remaining seven ν_1 cross-section data down to 325 nm (with the exception of one data point measured by Abe, Wakayama, and Ito,[13] which is clearly in error) indicates that the ν_1 neat cross section increases by 13–14 from 514 to 325 nm. We also measured the benzene ν_1 cross section at 514 and 325 nm in a solution 1% by volume benzene in acetonitrile, using the 918 cm^{-1} acetonitrile band dispersion as a reference,[4] and find a similar increase of 13 in the ν_1 cross section. Our vapor-phase A-term best fit to the six ν_1 cross-section data between 514 and 280 nm (Fig. 1) also gives an increase of 13 for the vapor between 514 and 325 nm. This value is inconsistent with the expected 15–20% increased condensed-phase dispersion over that of the vapor phase.

Schomaker, Delaney, and Champion[8] also measured several benzene ν_2 C–H stretching cross sections between 514 and 325 nm. We compare our ν_2 vapor-phase dispersion to their data by simply taking the ratio of their 325 nm/514 nm ν_2 cross sections of $(47.7 \pm 6.6)/(4.53 \pm 0.18)$ to give an increase of the neat ν_2 cross section from 514 to 325 nm of 10.6 ± 1.3. Our ν_2 benzene vapor-phase A-term best fit to the six 514–280 nm data gives a calculated dispersion of 11.0 between 514 and 325 nm. This vapor-phase dispersion again is identical to that in the liquid. To confuse any obvious conclusions it should be pointed out that our ν_1 and ν_2 vapor cross sections at 514 nm, when multiplied by $L_B \simeq 4.1$ (Table II), give neat cross-section values of 29 and 49 μb/sr, respectively. These values agree well with the average neat ν_1 cross section of 30 μb/sr,[8] and Schomaker, Delaney, and Champion's ν_2 514 nm cross section of 45 μb/sr.

The condensed-phase acetonitrile and cyclohexane Raman cross-section dispersion data in Figs. 3 and 4 also seem identical to the vapor dispersions. The curve in Fig. 3 derives from an A-term fit to the four I_R/I_L data points of the 2900–3000 cm^{-1} acetonitrile C–H stretching bands, giving $K_2 = 0$ and $\nu_e \equiv 110\,000$ cm^{-1}. This dispersion clearly also models the three cyclohexane 2800–3000 cm^{-1} C–H stretching data shown in Fig. 3. The cross sections of both liquid acetonitrile and liquid cyclohexane thus increase by ~ 70 between 514 and 230 nm. We compared the vapor phase the C–H stretching Raman cross sections of acetonitrile and cyclohexane to that of the 3060 cm^{-1} ν_2 C–H stretching mode of benzene at 514 and 230 nm. The acetonitrile and cyclohexane C–H cross sections both decreased by $\sim 10\%$ relative to the ν_2 benzene 3060 cm^{-1} band. The A-term fits to the benzene ν_2 vapor dispersions predicts an increase of ~ 80 for the ν_2 mode between 514 and 230, thus dispersions of ~ 70 for acetonitrile and cyclohexane vapor are indicated. These dispersions are identical to those of the liquids in Fig. 3. Once again the expected 15–25% increased dispersion from $L(\nu_0)$ (Table II) does not occur.

Figure 4 shows a cross-section increase for the benzene ν_2 C–H stretching mode of 75 for 40% benzene in liquid acetonitrile between 514 and 230 nm. This cross section increase is again essentially identical to the benzene ν_2 vapor results. In this case, a factor of 1.6 increase in the condensed-phase dispersion compared to the vapor is expected between 514 and 230 due to the dispersion in $L(\nu_0)$ (Table II). Even if the dispersion difference predicted by Eq. (4) for the acetonitrile 2942–3000 cm^{-1} band in pure acetonitrile versus 40% benzene in acetonitrile is assumed, the benzene ν_2 dispersion in Fig. 4 is still significantly less than the measured vapor dispersion plus the predicted dispersion from $L(\nu_0)$.

It should be pointed out that any similar comparison of the benzene ν_1 ring breathing-mode dispersion between 514 nm and wavelengths to the blue of the $^1B_{2u}$ transition in the vapor and the condensed phase is complicated by the significant condensed-phase redshift of the $^1B_{1u}/^1E_{1u}$ electronic states from which the ν_1 mode derives intensity. In this case, the change ν_e is not negligible compared to $\nu_e - \nu_0$, which makes conclusions on the manifestation of $L(\nu_0)$ (or lack of) difficult.

C. Lack of dispersion in the local-field effect

The direct comparison of condensed- and vapor-phase Raman cross-section dispersions for benzene, cyclohexane, and acetonitrile suggests that the dispersions in the condensed and vapor phase are identical. The expected additional dispersions from $L(\nu_0)$ are not observed. It is possible that this increased dispersion is fortuitously "counteracted" by changes in $\alpha_{\rho,\sigma}$, which occur in the opposite direction and of the proper magnitude for all three molecules studied, so as to give no net change in the condensed- versus vapor-phase dispersion. This scenario seems highly unlikely. A systematic underestimation of condensed-phase dispersions from the methodology of Dudik, Johnson, and Asher,[4] or a similar overestimation of the methane dispersion measured by Black and Bischel,[16] cannot explain the apparent lack of $L(\nu_0)$; the vapor- and condensed-phase dispersions are identical even for samples where the $L(\nu_0)$ dispersion would vary in value from 1.15 to 1.60. Additionally, both Black and Bischel's dispersions and those measured by the method of Dudik, Johnson, and Asher, as described in Fig. 3 agree with dispersion measurements by other workers. Black and Bis-

chel's methane dispersions give a benzene ν_1 vapor dispersion between 514 and 337 nm which is in good agreement with that measured in the vapor by Udagawa *et al.*[17] The method of Dudik, Johnson, and Asher gave a SO_4^{2-} 253.7 nm/435.8 nm cross-section ratio of 17, which agreed well with the value of 18 measured by Moser and Hoffman.[22] The ν_1 992 cm^{-1} cross-section increase between 514 and 325 nm we measured here of 13 in the 1% benzene in acetonitrile solution agrees with the measurements of Schomaker, Delaney, and Champion,[8] and supports the dispersion measurements of the 918 cm^{-1} acetonitrile band measured by Dudik, Johnson, and Asher.[4]

The liquid cyclohexane dispersions we measure in Fig. 3 significantly differ from those reported by Trulson and Mathies[7] between 547 and 239 nm. While our ultraviolet 2800–3000 cm^{-1} mode cyclohexane cross sections agree with theirs, our visible cross sections are substantially larger. At 514 nm, the relative intensity ratios of the ν_2 mode of benzene compared to that of cyclohexane, using either the benzene ν_2 cross-section data of Schomaker, Delaney, and Champion, or those derived from our acetonitrile data as described above, indicate that Trulson and Mathies' 514 cross-section value is a factor of ~ 2 too low. Indeed, Trulson and Mathies' own cross-section data at 532 nm, plus a simple ν_s^4 dependence, give a cross section at 514 nm, 1.6 times larger than they report.

We currently have no satisfactory explanation for the apparent lack of the additional dispersion from $L(\nu_0)$ in the condensed phase. Several solute–solvent systems have been reported which deviate from the behavior described by Eqs. (4) and (5) in the visible spectral region; the value of $\sigma_{mn}(\text{solution})/[\sigma_{mn}(\text{vapor}) \times L(\nu_0)]$ deviates from unity. These deviations have been ascribed to specific intramolecular interactions such as hydrogen bonding, which invalidate the continuum dielectric model leading to Eqs. (4) and (5). However, even in the presence of such interactions, by simply changing the excitation wavelength and thus the values of n, n', n_{sol}, and n'_{sol}, one would expect the same proportional deviation, and thus the predicted $L(\nu_0)$ dispersion. Whatever the case, the data here indicate that the predicted dispersion in $L(\nu_0)$ should no longer be assumed in condensed-phase preresonance Raman cross-section studies. These results may have an impact on trying to relate chromophore Raman intensities to environment through the "microscopic" refractive index and expressions such as Eq. (4). These results are important enough that further investigations comparing condensed- and vapor-phase Raman cross-section dispersions are warranted.

V. CONCLUSIONS

The gas-phase Raman cross-section dispersion of the benzene ν_1 992 cm^{-1} ring breathing mode at wavelengths longer than 280 nm is described by the A-term expression with $\nu_e \simeq 75\,000$ cm^{-1}. At shorter wavelengths, the ν_1 mode dispersion is dominated by enhancement from the $^1B_u/^1E_{1u}$ electronic states near 55 000 cm^{-1}. The benzene ν_2 3060 cm^{-1} carbon–hydrogen stretching vibration dispersion between 514 and 220 nm is described by an A-term expression with $\nu_e \simeq 105\,000$ cm^{-1}, indicating no enhancement of the dipole-allowed $^1E_{1u}$ transition. Detailed comparison of these vapor-phase dispersions to previously measured condensed-phase benzene dispersion measurements, as well as comparisons between acetonitrile and cyclohexane vapor and liquid dispersions, do not reveal the expected increase in the condensed-phase dispersions due to the dispersion in the local electromagnetic field. Our results indicate that the conventional expectation of the impact of the dielectric environment on the Raman cross-section dispersion is incorrect.

ACKNOWLEDGMENT

We gratefully acknowledge support of this work from NIH Grant No.IR01GM30741-08.

[1] A. C. Albrecht, J. Chem. Phys. **34**, 1476 (1960).
[2] A. C. Albrecht and M. C. Hutley, J. Chem. Phys. **55**, 4438 (1971).
[3] See, for example, J. Tang and A. C. Albrecht, *Raman Spectroscopy, Theory and Practice*, edited by H. A. Szymanski (Plenum, New York, 1970), Vol. II.
[4] J. M. Dudik, C. R. Johnson, and S. A. Asher, J. Chem. Phys. **82**, 1732 (1985).
[5] L. Ziegler and A. C. Albrecht, J. Chem. Phys. **67**, 2753 (1977).
[6] J. M. Dudik, C. R. Johnson, and S. A. Asher, J. Phys. Chem. **89**, 3805 (1985).
[7] M. O. Trulson and R. A. Mathies, J. Chem. Phys. **84**, 2068 (1986).
[8] K. T. Schomacker, J. K. Delaney, and P. M. Champion, J. Chem. Phys. **85**, 4240 (1986).
[9] S. A. Asher and C. R. Johnson, J. Phys. Chem. **89**, 1375 (1985).
[10] G. Eckhardt and W. Wagner, J. Mol. Spectrosc. **19**, 407 (1966).
[11] G. Fini, P. Mirone, and P. Patella, J. Mol. Spectrosc. **28**, 144 (1968).
[12] J. R. Nestor and E. R. Lippincott, J. Raman Spectrosc. **1**, 305 (1973).
[13] N. Abe, M. Wakayama, and M. Ito, J. Raman Spectrosc. **6**, 38 (1977).
[14] H. W. Schrötter and H. W. Klöckner, in *Topics in Current Physics*, Vol. 4, edited by A. Weber (Springer-Verlag, Berlin, 1979), p. 123.
[15] S. A. Asher, C. R. Johnson, and J. Murtaugh, Rev. Sci. Instrum. **54**, 1657 (1983).
[16] G. Black and W. K. Bischel, in *Excimer Lasers*, edited by C. K. Rhodes, H. Egger, and H. Pummer (American Institute of Physics, New York, 1983).
[17] Y. Udagawa, N. Mikami, K. Kaya, and M. Ito, J. Raman Spectrosc. **1**, 341 (1973).
[18] P. A. Harmon and S. A. Asher, J. Chem. Phys. **88**, 2925 (1988).
[19] E. E. Koch and A. Otto, Chem. Phys. Lett. **12**, 476 (1972).
[20] M. B. Robin, in *Higher Excited States of Polyatomic Molecules* (Academic, New York, 1985), Vol. III.
[21] B. L. Sowers, E. T. Arakawa, and R. D. Birkhoff, J. Chem. Phys. **54**, 2319 (1971); B. L. Sowers, M. W. Williams, R. N. Hamm, and E. T. Arakawa, J. Chem. Phys. **57**, 167 (1972).
[22] W. Hofman and H. Moser, Bunsenges. Phys. Chem. **68**, 129 (1964).